Analyst

Accepted Manuscript

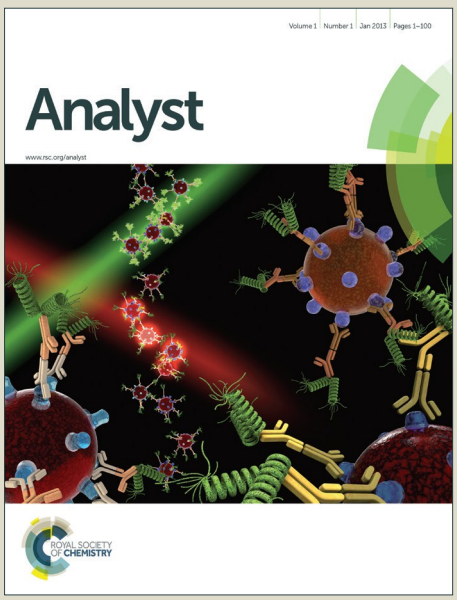

ROYAL SOCIETY OF CHEMISTRY

www.rsc.org/analyst

Journal Name

ARTICLE

Received 00th January 20xx,
Accepted 00th January 20xx
DOI: 10.1039/x0xx00000x
www.rsc.org/

Immobilization of Multivalent Glycoprobes on Gold Surfaces For Sensing Proteins and Macrophages.

Madhuri Gade,[a] Puneet Khandelwal,[b] Sivakoti Sangabathuni,[a] Harikrishna Bavireddi,[a] Raghavendra Vasudeva Murthy, [a] Pankaj Poddar,[b] and Raghavendra Kikkeri*[a]

Multivalent display of carbohydrates on cell surface provides cooperative binding to improve the specific biological events. In addition to multivalency, spatial arrangement and orientation of sugars with respect to external stimuli also trigger carbohydrate-protein interactions. Herein, we report non-covalent host-guest strategy to immobilize heptavalent glyco-β-cyclodextrin on gold-coated glass slides to study multivalent carbohydrate-protein interactions. We have found that the localization of sugar entities on surfaces using β-cyclodextrin (**β-CD**) chemistry increased the avidity of carbohydrate-protein and carbohydrate-macrophages interactions as compared to monovalent-**β-CD** sugar coated surfaces. This platform is expected to be a promising tool to amplify the avidity of sugar-mediated interactions on surfaces and contribute to the development of next generation bio-medical products.

Introduction

Carbohydrates are recognized as information-rich biomolecules that play an important role in the human body. The surface of all mammalian cells is covered with carbohydrates that are attached to proteins and lipids embedded on the cell membrane. The interaction with the extracellular world is achieved through interaction between these carbohydrates and carbohydrate-binding proteins (lectins) which are present on surfaces of other mammalian cells, viruses, bacteria and bacterial toxins.[1] To enhance the strength of cell surface binding, nature often assembles multiple protein-carbohydrate complexes to provide the necessary avidity. The effect of multivalency concerning sugars present on surfaces as compared to monovalancy has been described by several investigators [2-3] and was found to be of critical importance in the field of protein-carbohydrate interactions. In addition to increase in avidity, multivalency enhances the selectivity of a particular interaction and amplifies small differences in the intrinsic binding avidity.[4-5] Recently, the effort has been initiated to synthesize multivalent probes using peptides,[6] polymers,[7] dendrimers,[8-9] nanoparticles and supramolecular complexes,[10] for studying the carbohydrate-protein interactions in solution based techniques.[11-13] Alternatively, surface immobilization of monovalent sugars present multivalent arrays to facilitate the analysis of lectin binding and can be relevant to the cell surface carbohydrate presentation.[14-19] To date, there are several methods reported to immobilize carbohydrates in an array format to study carbohydrate-lectin interactions. Carbodiimide coupling procedure is a well-studied technique that yield glycan arrays for evaluating high-throughput analysis.[20-22] Thiol-ene/-yne reactions were used to evaluate lectin-carbohydrate binding by quartz crystal microbalance (QCM) flow-through instrument.[23] Other techniques described in the literature include boronic acid-diol interaction, maleimido-thio interaction, click reactions, Staudinger reaction and epoxide-amine reaction.[24-27] Although these methods can improve the immobilization of carbohydrates on the surfaces, it is still limited by the orientation, spatial arrangement and local concentration of sugars on the surfaces to increase the avidity of specific carbohydrate-protein interactions.[28] Recently, host-guest interactions such as those of β–cyclodextrin (**β–CD**) systems have proven to be important for constructing patternized surfaces.[29-32] The advantage of host-guest method is that they can provide structural versatility and localized sugar concentration. More importantly, they have been used as a regeneration platform with high reproducibility for continuous modification of same sugar or different sugar substrates to study the interaction with different glycoproteins and bacteria.[33-36] This method can be used in the point of care devices.

With the goal of creating multivalent carbohydrate surfaces, we report here **β-CD**-based host-guest scaffold which is synthetically facile and also displays localized multivalent carbohydrates. The technique that we report includes immobilization of PEGylated adamantyl molecule (AD) to serve as a linker by a simple self-assembly process, followed by its formation of strong host-guest complexes with **β–CD** derivatives that were modified by attaching mannose residues (scheme 1). The existence of host-guest complexes on the gold substrates was characterized by surface analysis techniques. A combination of surface plasmon resonance (SPR) and THP-1 differentiated macrophage binding assay were employed to demonstrate the advantage of multivalent carbohydrate-protein interactions on the surfaces. The rationale for choosing Concanavalin A (**Con A**) lectin is due to its selective binding with mannose or glucose sugars. The significant advantage of this approach is the simplicity of integrating a system with multivalent carbohydrate aggregates that interact with lectins and cells. Such a system is essential for tuning the selectivity and sensitivity of the specific carbohydrate-protein interactions.

Materials and methods

General Information.

All chemicals were of reagent grade and unless otherwise noted were used as supplied. TLC was performed on Merck silica gel 60 F254 plates (0.25 mm) and visualized by UV or by dipping the plate

[a]*Indian Institute of Science Education and Research, Pashan, Pune 411008, India. Fax: +91-20-25899790; Tel: +91-20-25908207; E-mail: rkikkeri@iiserpune.ac.in*
[b]*Physical and Material Chemistry, CSIR-National Chemical Laboratory, Dr. HomiBhabha Road, Pune-411008, India.*

† Electronic Supplementary Information (ESI) available: [details of any supplementary information available should be included here]. See DOI: 10.1039/x0xx00000x

in CAM/ninhydrin solution and heating. Column chromatography was carried on Fluka Kieselgel 60, mesh 230–400. ^{1}H and ^{13}C NMR spectra were recorded on Jeol 400 MHz. Chemical shifts (δ) are reported in ppm, coupling constants (J) in Hz. Residual solvents, for $CDCl_3$ - δ_H, 7.26 and δ_C 77.3, for CD_3OH. δ_H 3.31, and δ_C 49.0, D_2O - δ_H, 4.75, were used as internal references.

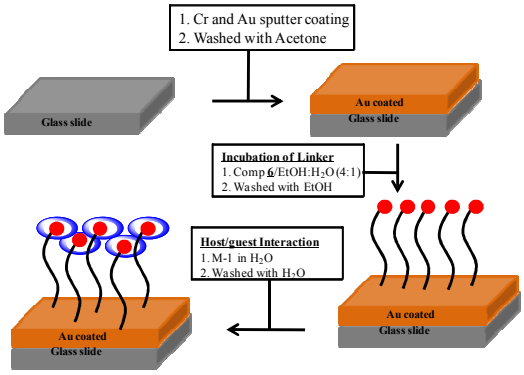

Scheme 1. Schematic of the different steps to immobilize supramolecular scaffold on gold coated glass slides.

.

Experimental Details.

2-(2-(2-(undec-10-en-1-yloxy)ethoxy)ethoxy)ethanol (**1**).

2,2'-(ethane-1,2-diylbis(oxy)bis(ethan-1-ol) (5 ml, 29.90 mmol) and 11-bromoundec-1-ene (2.61 ml, 11.96 mmol) were dissolved in THF (10 ml) and the solution was cooled to 0°C. Sodium hydride (0.29 g, 11.96 mmol) was added. The reaction mixture was warmed to 22 °C and allowed to stirr for 12 hours. Water (10 ml) was slowly added to quench the excess of base. The solution was extracted with DCM (25 ml) and the aqueous phase was washed 3 times with EtOAc (3×50 mL). The combined organic layer was dried over Na_2SO_4 and concentrated under reduced pressure. The residue was purified by flash column chromatography (silica gel, pet ether/EtOAc 1:8). The solvent was removed using reduced pressure and the product was dried with high vacuum. The product 2-(2-(2-(undec-10-en-1-yloxy)ethoxy)ethoxy)ethanol (**1**) was obtained as oil (5.96 g, 60% yield). ^{1}H NMR (400 MHz, $CDCl_3$): δ 5.87-5.77 (m, 1H), 5.02-4.92 (m, 2H), 3.75-3.58 (m, 12H), 3.46 (t, J = 6.41 Hz, 2H), 2.07-2.01 (m, 2H), 1.62-1.55 (m, 2H), 1.36-1.26 (m, 12H).^{13}C NMR (100 MHz, $CDCl_3$): δ 139.13, 114.02, 72.47, 71.50, 70.51, 70.23, 69.91, 61.60, 33.72, 29.46, 29.44, 29.37, 29.34, 29.02, 28.83, 25.96. HRMS (ESI) m/z: calc'd for $C_{17}H_{34}O_4Na$, 325.2354; Found, 325.2357.

T*ert*- butyl 4, 7, 10, 13-tetraoxatetracos-23-enoate (**2**). Compound **1** (0.5 g, 1.65 mmol) was dissolved in THF (5 ml), a catalytic amount of potassium *tert*-butoxide (0.05 g, 0.45 mmol) was added followed by dropwise addition of *tert*-butyl acrylate (0.21 ml, 1.65 mmol). The reaction mixture was stirred at room temperature for 16 h and neutralized with 1M HCl. The solvent was removed and the oily residue was taken up in brine (30 ml) and extracted with EtOAc (3×15 ml). The combined organic layer was washed with brine (50 ml) and dried over Na_2SO_4. The solvent was removed in vacuo, and the residue was purified by column chromatography (silica gel, pet ether/ EtOAc 1: 8). T*ert*- butyl 4, 7, 10, 13-tetraoxatetracos-23-enoate (**2**) was obtained as oil (0.73 g, 85% yield). ^{1}H NMR (400 MHz, $CDCl_3$): δ 5.84-5.75 (m, 1H), 5.01-4.90 (m, 2H), 3.71 (t, J = 6.87 Hz, 2H), 3.65-3.56 (m, 12H), 3.44 (t, J = 6.87 Hz, 2H), 2.50 (t, J = 6.41 Hz, 2H), 2.06-1.98 (m, 2H), 1.60-1.53 (m, 2H) 1.44(s, 9H), 1.36-1.27 (bm, 12H); ^{13}C NMR (100 MHz, $CDCl_3$): δ 170.88, 139.18, 114.07, 80.45, 71.50, 70.57, 70.47, 70.34, 70.01, 66.86, 36.22, 33.77, 29.58, 29.50, 29.43, 29.39, 29.08, 28.89, 28.05, 26.04. HRMS (ESI) m/z: calc'd for $C_{24}H_{46}O_6Na$, 453.3192; Found, 453.3190.

4, 7, 10, 13-tetraoxatetracos-23-enoic acid (**3**). Compound **2** (0.4 g, 0.93 mmol) was dissolved in MeOH:THF (8 ml, 1:1). Aqueous 4M NaOH (3 ml, 12 mmol) was added and the solution was stirred at room temperature for 4 h. The solvent was removed under reduced pressure and the resulting suspension was acidified with aqueous 6M HCl (4 ml) while cooling at 0 °C. DCM (50 ml) was added and the organic layer was separated and dried over Na_2SO_4. Removal of the solvent and after drying yielded compound **3** as oil (0.24 g, 70% yield). ^{1}H NMR (400 MHz, $CDCl_3$): δ 5.85-5.77 (m, 1H), 5.00-4.90 (m, 2H), 3.76 (t, J = 5.95 Hz, 2H), 3.65-3.58 (m, 12H), 3.45 (t, J = 6.87 Hz, 2H), 2.62 (t, J = 5.95 Hz, 2H), 2.04 (q, J = 7.33 Hz, 2H), 1.59-1.54 (m, 2H), 1.36-1.25 (bm, 12H); ^{13}C NMR (100 MHz, $CDCl_3$): δ 175.55, 139.17, 114.05, 71.51, 70.57, 70.50, 70.41, 70.20, 69.95, 66.39, 34.90, 33.75, 29.63,29.47, 29.43, 29.38, 26.06, 28.86, 25.96. HRMS (ESI) m/z: calc'd for $C_{20}H_{39}O_6$, 375.2746; Found, 375.2742.

N-(adamantan-1-yl)-3-(2-(but-3-en-1-yloxy)ethoxy)propanamide (**4**). Compound **3** (0.34 g, 0.90 mmol) and adamantan-1-amine (0.15 g, 0.90 mmol) were dissolved in DMF (10 ml) then HOBt (0.15 g, 1.09 mmol), EDC (0.20 g, 1.09 mmol) and DIPEA (0.39 ml, 2.25 mmol) were added. The reaction mixture was stirred for 24 h. DMF was evaporated under reduced pressure. The residue was taken up in 30 ml of brine and extracted 3 times with 15 ml of EtOAc. The combined organic layer was washed with 50 ml brine and dried over Na_2SO_4. The solvent was removed in vacuo, and residue was purified column chromatography (silica gel, pet ether/ EtOAc 1:8) and dried under reduced pressure and high vacuum to give the corresponding **4** (0.36 g, 80%) as oil. ^{1}H NMR (400 MHz, $CDCl_3$): δ 6.13(bs, 1H), 5.85-5.77 (m, 1H), 5.02-4.92 (m, 2H), 3.68 (t, J = 5.95 Hz, 2H), 3.66-3.58 (m, 12H), 3.45 (t, J = 6.87 Hz, 2H), 2.39 (t, J = 5.95 Hz, 2H), 2.04-2.03 (bm, 5H), 1.98 (bs, 6H), 1.67 (bs, 6H), 1.59-1.54 (m, 2H), 1.36-1.26 (m, 12H); ^{13}C NMR (100 MHz, $CDCl_3$): δ 171.13, 139.22, 114.10, 71.57, 70.63, 70.55, 70.40, 70.33, 70.01, 67.52, 51.78, 41.50, 36.34, 33.79, 29.59, 29.53, 29.45, 29.39, 29.11, 28.91, 26.06. HRMS (ESI) m/z: calc'd for $C_{30}H_{53}NaO_5N$, 530.3821; Found, 530.3810.

S-(2-(2-(2-(3-(adamantan-1-ylamine)-3-oxopropoxy)ethoxy)ethoxy) ethyl) ethanethioate (**5**). Compound **4** (0.25 g, 0.49 mmol) and AIBN (0.49 g, 2.95 mmol) were dissolved in dioxane (7 ml). Thioacetic acid (0.90 ml, 12.81 mmol) was added and the solution was stirred for 12 h at 60 °C. The solvent was removed and the crude was purified by flash column chromatography (silica gel, pet ether/EtOAc 1:1 to 1:9) and dried to give the product **5** as yellowish oil (0.13 g, 47% yield). ^{1}H NMR (400 MHz, $CDCl_3$): δ 6.02(bs, 1H), 3.69 (t, J = 5.95 Hz, 2H), 3.65-3.56 (m, 12H), 3.44 (t, J = 6.87 Hz, 2H), 2.85 (t, J = 7.33 Hz, 2H), 2.37 (t, J = 5.95 Hz, 2H), 2.32 (s, 3H), 2.06-2.05 (bm, 3H), 1.99 (bm, 6H), 1.67 (bs, 6H), 1.58-1.53 (m, 4H), 1.28-1.25 (bm, 14H); ^{13}C NMR (100 MHz, $CDCl_3$): δ 196.05, 170.67, 71.52, 70.60, 70.53, 70.39, 70.31, 69.99, 67.58, 51.59, 41.54, 38.10, 36.35, 30.60, 29.57, 29.45, 29.38, 29.10, 29.06, 28.76, 26.03. HRMS (ESI) m/z: calc'd for $C_{32}H_{58}SO_6$, 584.3985; Found, 584.3993.

N-(adamantan-1-yl)-3-(2-(4-ercaptobutoxy)ethoxy)propanamide (**6**). Compound **5** (0.15 g, 0.26 mmol) was dissolved in MeOH (7 ml). Sodium methoxide (0.066 g, 1.28 mmol) was added and the reaction was stirred at RT for 1 hour. The solution was neutralized with Resin Amberlite H^+ IR 120. The polymer was filtered through filter paper and washed with MeOH (15 ml). The solvent was removed under reduced pressure and the residue was dried under high vacuum to give the **6** as yellowish oil (0.12 g, 93% yield). ^{1}H NMR (400 MHz, $CDCl_3$): δ 6.00(S, 1H), 3.6 (t, J = 5.95 Hz, 2H), 3.63-

3.54 (m, 12H), 3.42 (t, J = 6.87 Hz, 2H), 2.67-2.63 (m, 1H), 2.52-2.46 (m, 1H), 2.35 (t, J = 5.95 Hz, 2H), 2.03(bs, 3H), 1.79 (bs, 6H), 1.64 (bs, 6H), 1.58-1.51 (m, 2H), 1.36-1.24 (bm, 16H); ^{13}C NMR (100 MHz, $CDCl_3$): δ170.62, 71.52, 70.57, 70.52, 70.37, 70.28, 69.96, 67.58, 51.56, 41.52, 38.11, 36.34, 29.56, 29.43, 29.37, 29.19, 28.47, 26.03. HRMS (ESI) m/z: calc'd for $C_{30}H_{56}NSO_5$, 542.3878; Found, 542.3875.

Mono-mannose substituted β-cyclodextrin (**M-2**). Compound **7** (100 mg, 1.15 mmol), mannose alpha propargyl (10 mg, 1.73 mmol), sodium ascorbate (3 mg, 14.7 µmol) and copper(II) sulfate pentahydrate (2 mg, 7.3 µmol) were suspended in 5 mL dimethylformamide in a round bottom flask and stirred at RT overnight. The solvent was evaporated and the product was purified by sephadex column using pure water as a solvent yielded (32 mg, 27%) of **M-2** ^{1}H NMR (400 MHz, MeOD-d_4) δ 7.39 (bs, 1H), 4.94 (bs, 7H), 3.97-3.33 (m, 72H), ^{13}C NMR (100 MHz, $CDCl_3$): 130.5, 129.4, 101.9 (anomeric-C), 99.6, 80.9, 73.2, 72.1, 71.3, 69.5, 63.3, 60.1, 59.7 MS (MALDI–TOF) m/z calc'd for $C_{51}H_{83}NaN_3O_{40}$, 1400.4451; Found 1400.8681.

Surface Functionalization. *Preparation of adamantyl monolayer:* Glass slides (approx. 1x1 cm) were washed with EtOH and coated with a gold substrate (100 nm) using gold evaporation chamber (Minilab deposition system type ST80A, UK) at a pressure of about 4x10^{-6} mbar. Samples were immersed in an ethanolic solution of **6** (0.2, 0.02 and 0.005 M) for 48 h. The adamantyl coated glass slides were rinsed with ethanol and stored at controlled conditions.

Immobilization of cyclodextrin derivatives: The gold substrate (modified with adamantyl SAM) was washed twice with ethanol and immersed in a solution of **M-1** (10 µM solution in deionized water) for 24 h. The samples were rinsed with water, dried under a stream of nitrogen, and used as such for contact angle, ellipsometry and AFM measurements.

Lectin immobilization: The gold substrate (modified with **M-1**) was immersed in a solution of **Con A** lectin (1 mg/1ml in 10mM HEPES, 150 mM NaCl, 2mM $CaCl_2$, 2mM $MnCl_2$, pH7.3) for 1 h and washed with water and dried under nitrogen. The substrates were used as such for ellipsometry, and AFM measurements.

Contact angle measurements. Contact angle analyses were performed using optical contact angle apparatus (Holmarc's HO-IAD-CAM-01) equipped with a CCD camera and high performance aberration corrected imaging with precise manual focus adjustment. Image J software was used for data acquisition. Rectangular gold coated substrates were fixed and kept constant throughout the analysis by means of sample holder. The contact angle of water in air was measured by the sessile drop method by gently placing a drop of 4 µL of Milli-Q water onto the coated surface. The whole analysis was conducted at room temperature. A minimum of 20 droplets were examined for each surface. The resulting mean contact angle value was used for the following calculations.

Spectroscopic ellipsometry. The thicknesses of the **6** (0.02 M), **6/M-1** (0.02 M/10 µM) and **6/M-1/Con A** (0.02 M/10 µM/1 mg/mL) coated glass slides were measured by a commercial spectroscopic ellipsometer (M2000 from Woollam Inc., Lincoln, Nebraska) in the transmission mode in a spectral range from 250 to 800 nm with the compensator making 100 rev/s. Measurements were recorded at various angles of incidence between 60^o to 70^o. A four-layer model (Au coated BK7 glass substrate and three successive organic layers) was used in the fitting with WVASE software to obtain the thickness of the layers of **6**, **M-1** and **Con A** from the measured Ψ and Δ curve.

The Ψ and Δ values are related to the reflection coefficients as

$$\tan(\Psi).e^{i\Delta} = \frac{R_p}{R_s} = \rho(\lambda, d, N) \quad \text{--------(1)}$$

Where Rp and Rs are the reflection coefficients of p- and s-polarized light, λ is the wavelength of the incident light, d is the thickness of the film and N is the complex refractive index. The complex function ρ is ratio of amplitude Ψ and phase difference Δ between the p- and s- polarized light waves. Equation 1 was used for the fitting of ellipsometric data. The best fit to the experimental data was determined by minimizing the mean-square error (MSE)[2] where K is the number of (Ψ, Δ) pairs, M is the number of the model parameters, and the mod and exp refer to model and experimental values, respectively.

$$MSE = \frac{1}{2K-M} + \sum_{j=1}^{k}[(\Psi_j^{mod} - \Psi_j^{exp})^2 + (\Delta_j^{mod} - \Delta_j^{exp})^2 \quad \text{--(2)}$$

The Ψ and Δ curve measurements were performed in 4 sets: (a) **Au**, (b) **6/Au**, (c) **Au/6/M-1** and (d) **Au/ 6/M-1/Con A** coated glass slides. As Δ values are very sensitive to the film thickness, in **Figure 2**, we have plotted Δ vs. λ curves for an angle of incidence of 60° for all the samples. These curves clearly indicate the decrease in the Δ values upon increase in the film thickness (i.e. from bare Au coated glass slide to **Au/6/M-1/Con A** coated glass slides). Since the Au film deposited on glass plate was opaque, the thickness of Au film was ignored and was taken as an infinitely absorbing material. Therefore, only the optical constants of Au were considered for fitting. The corresponding Ψ and Δ curves are presented in **Figure S1a** and **S1e**, respectively. The ellipsometry data for organic layers were fitted using a Cauchy model layer which is quite well acceptable for transparent films. For Cauchy layers, the data was fitted for thicknesses only. The thickness for **6**, **6/M-1** and **6/M-1/Con A** layers were measured to be 13.9 Å , 29.82 Å and 92.93 Å, respectively. **Figure S1** compares between experimental and modeled Ψ and Δ curves for **6**, **6/M-1** and **6/M-1/Con A** films, respectively. **Figure S1** shows that Ψ curve fits "degrade" as the thickness grows, which suggests that either the microstructure of the "film" is not optically smooth and/or the film has some absorption in the measured wavelength range. However, Δ curve fit shows a good agreement with the experimental data throughout the wavelength range. Error bar represent fitting standard deviation for each measurement.

Estimation of concentration of sugar on slide. The concentration of mannose sugar on gold coated glass slides were determined by the phenol-sulfuric acid method. A sugar functionalized-glass slide was dipped in concentrated sulfuric acid (750 µL, 100%) and aqueous phenol solution (5% w/v, 100 µL) was added to the test tube and heated to 80°C. After 5 min, the Au-slides were removed and cooled to room temperature. The absorbance coefficient at 490 nm was measured. The sugar concentration was estimated by comparing the absorption of the sample with a standard curve.

X-ray photoelectron spectroscopy. XPS experiments were performed on a VG Micro Tech ESCA 3000 instrument at a pressure of < 1x10^{-9} Torr. The overall resolution was limited to the bandwidth of X ray source (~ 1 eV). The spectra were recorded with monochromatic Al Kα radiation at pass energy of 50 eV and an electron take off angle of 60^o. C 1s energy binding peaks centered at 284.6 eV was used for calibration. The deconvolution of the XPS peaks was done by a XPS peak fitting program (XPSPEAK 4.1). The XPS spectra were background corrected using the Shirley algorithm, and chemically distinct peaks were resolved using a nonlinear least-square fitting procedure.

Atomic force microscopy. Atomic force microscopy (AFM) measurements were performed with Au coated glass slides with **6**,

with **6/M-1** and with **6/M-1 /Con A** using a Multimode scanning probe microscope equipped with a Nanoscope IV controller from Veeco Instrument Inc., Santa Barbara, CA. All AFM measurements were done under ambient conditions using the tapping-mode AFM probes model Tap190Al purchased from Budget Sensors. The radii of tips were less than 10 nm, and their height was ~ 17 µm. The cantilever' resonant frequency was ca. 162 kHz and nominal spring constant of ca. 48 N/m, with a 30 nm thick aluminum reflex coating on the back side of the cantilever of the length 225 µm. For each sample, three locations with a surface area of 1×1 μm^2 and 500 × 500 nm^2 each were imaged at a rate of 1 Hz and at a resolution of 512×512.

Surface Plasmon Resonance study. Binding kinetics was determined by SPR using a BIACORE 300 biosensor instrument (GE Biosystems). Concavalin A was purchased from Sigma-Aldrich. The gold sensor chip and different running buffers were obtained from GE Healthcare Life Science (India). All SPR experiments were performed using Biacore 3000. For the preparation of host-guest coated surfaces, gold sensor chip was activated with **6** (0.01 mM or 0.1 mM) injected at a flow rate 10 µl min^{-1} for 3 minutes which resulted in adamantyl coated surface for host-guest functionalization. Finally, cyclodextrin moiety was incorporated on adamantyl surface by injecting **M-1** or **M-2** or **β-CD** (0.05 mM or 0.5 mM) at a flow rate of 5 µl·min^{-1} for 7 minutes. This was followed by injecting **Con A** (0.5, 1.0, 2.5, 3.5 µM in 10mM HEPES, 150mM NaCl, 2mM $CaCl_2$, 2mM $MnCl_2$, pH7.3) for 250 s at 10 µL·min^{-1}, followed by dissociation using buffer at 30 µL·min^{-1} for 200 s. The equilibrium dissociation constant (K_D) was determined globally by fitting to the kinetic simultaneous K_a/K_d model, assuming Langmuir (1:1) binding, using BIA evaluation software (BIAcore). The surfaces were strictly regenerated with multiple pulses of α-D-methyl mannose followed by an extensive wash procedure using running buffer.

THP-1 differentiated Macrophage Binding Assay. Human THP-1 monocytic cell line (from NCCS, Pune) was grown at 37 °C and 5% CO_2 in RPMI-1640 (Invitrogen) medium with 10% heat inactivated FBS, 50 µg/mL streptomycin and 100 µg/mL penicillin (pH 7.2). THP-1 cells were differentiated by stimulating with PMA (10 ng/mL = 16 nM; from Sigma Aldrich, St Louis, MO, USA) for 3-4 days. Cells were detached by treating with 0.05% trypsin/EDTA solution. THP-1 derived macrophage cells were seeded on **6/ β -CD**, **6/M-1** and **6/M-2** coated plates at a density of 5000 cells/cm^2. After 24 h of incubation, slides were gently rinsed thrice with PBS to remove the unbound cells. The bound cells were imaged by using normal bright field microscopy.

Results and Discussion

The chemical structures of the molecules used for the formation of the self-assembled glycoclusters (**M-1**, **M-2**, and **6**) are depicted in fig. 1. The adamantyl derivative (AD) **6** was prepared in several steps, starting from conjugation of triethylene glycol with 11-bromoundec-1-ene, followed by its reaction with *t*-butyl acrylate to yield compound **2**. After hydrolysis with NaOH, the carboxylic acid **3** was obtained and coupling with 1-adamantylamine yielded adamantyl derivative **4**. The compound was treated with thioacetic acid and azoisobutyronitrile (AIBN), followed by deacetylation with NaOMe to yield compound **6** (Fig. 1). Mannose modified ***β*-CD** derivatives (**M-1)** were synthesized as described by García-Barrientos.[37] Mono-mannose substituted ***β*-CD** (**M-2**) was prepared by click reaction between CD-mono azide and propargyl mannoside. Robust adamantyl-based monolayers were formed by assembling linker **6** on gold-coated glass slides. Glass slides (approx. 1x1cm) were washed with EtOH and coated with chromium (10 nm) then with gold (100 nm) using gold evaporation chamber at a pressure of about $4x10^{-6}$ mbar. Samples were immersed in an ethanol solution of **6** (0.2, 0.02 and 0.005 M) for 48 h. The adamantyl coated glass slides were then rinsed with ethanol to remove physisorbed materials (Scheme 1) and were stored at controlled conditions. Monolayers were characterized by a combination of methods, namely, aqueous contact angles, atomic force microscopy (AFM), ellipsometry and X-ray photoelectron spectroscopy (XPS) (Fig. 3). Contact angle measurements revealed a 60^O angle for the freshly cleaned gold substrate which shifted to 64^O , 78^O and 85^O for the adamantyl monolayer surface (in 0.005, 0.02 and 0.2 M ethanolic solution of **6** respectively), reflecting the hydrophobic character of the surface.

The thickness of **6** (0.02 M) monolayer, measured by ellipsometry, was ~13.9 **Å** (Table 1, Entry 1, and Fig. S1, S1b & 1f), which is in good agreement with the values described for similar linker models in literature.[38] AFM images of the bare gold surfaces were relatively homogeneous with some nodules whereas gold-coated glass slides monolayered of **6** showed rough surface. The root-mean-square surface roughness (R) was found to be ~ 1.4 nm (Fig. 2b).

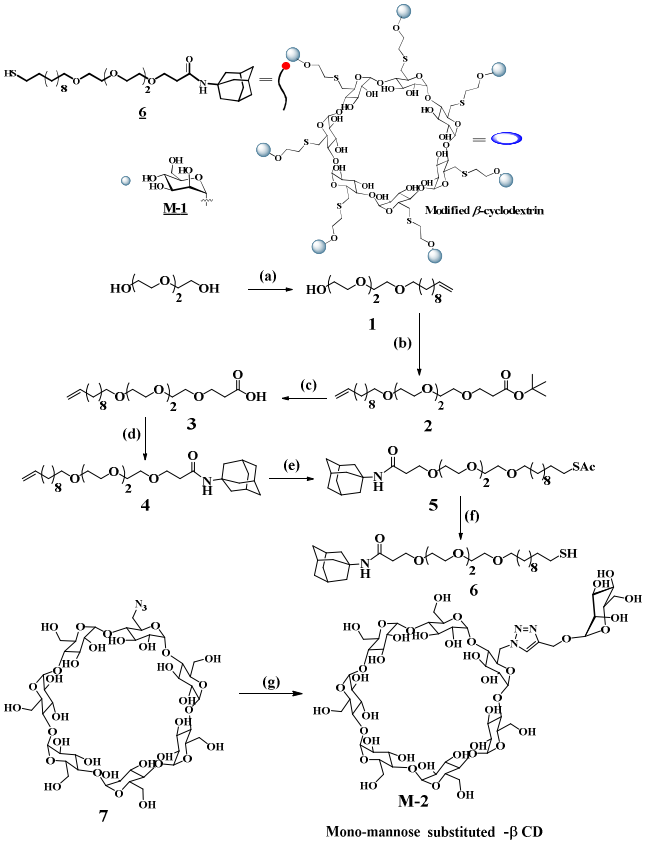

Fig. 1 Molecular structures and synthesis and their synthesis :(a) NaH, THF, 11-bromoundec-1-ene, 0 °C to 22 °C, 12h, 60%; (b) KO^tBu, THF, *tert*-butyl acrylate, rt, 16 h, 85%; (c) 4M NaOH, THF:MeOH (1:1), 4 h, 70%; (d) Adamantane amine, EDC, HOBt, DIPEA, DMF, 24 h, 80%; (e) AIBN, AcSH, Dioxane, 60 °C, 12 h, 47%; (f) NaOMe, MeOH, rt, 1 h, 85%, (g) $CuSO_4.5H_2O$, ascorbic acid, propargyl mannoside; H_2O, 60%.

The host-guest complex was prepared by the formation of complexes between ***β*-CD** and the adamantyl residues found as monolayers on the gold substrates. Freshly prepared adamantyl monolayers (prepared from 0.2, 0.02 M and 0.005 M solutions) were immersed in a solution of **M-1** (10 µM) for 24 hours at RT. The functionalized substrates were rinsed with deionized water to remove physisorbed materials and the contact angles were measured. The results indicated that the concentration and spatial arrangement of **6** dictates the number of complexes on the gold surface. As expected, 0.2 M of **6** resulted weak host-guest interaction due to the dense coating of hydrophobic adamantyl moiety, whereas 0.02 and 0.005 M of **6** resulted in a strong host-guest interaction, indicating that the host-guest interactions are better when the adamantyl units are distant from each other. This was further supported by phenol-sulfuric acid analysis of mannose concentration.

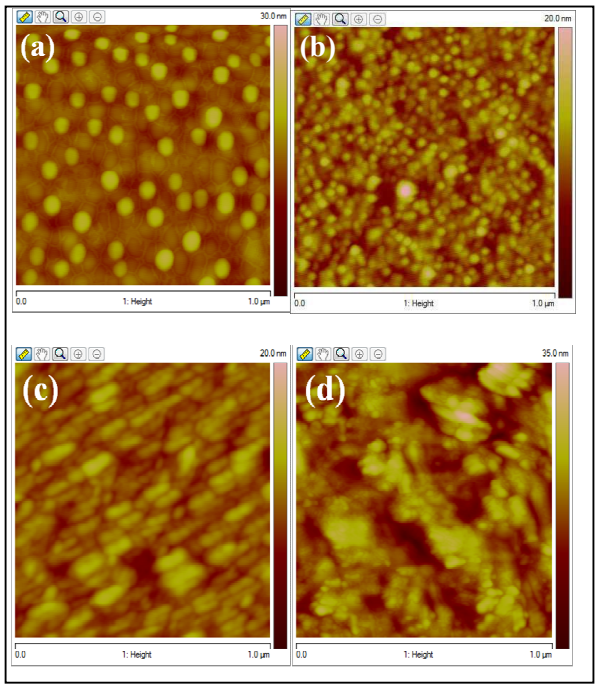

Fig. 2 AFM images of the different surfaces: (a) bare Au, (b) Au substrate coated with **6** (0.02 M); (c) **6/M-1** (0.02 M/10 µM) coated Au substrate and (d) **6/M-1/Con A** (0.02 M/10 µM/1 mg/mL) coated Au substrate.

A similar observation was described by Park *et al.*[39] For our experiment, we selected 0.02 M solution of linker **6** to avoid non-specific interactions between vacant gold surface and proteins or cells. The thickness of the film, after formation of the complexes, as indicated by ellipsometric measurements, increased to 29.82 Å (Table 1 Entry 2, Fig. S1, S1c & 1g), which is 2-fold more than that of the layer before the formation of the host-guest complex and it reflects the thickness of the ***β*-CD** moiety. The presence of the complexes on the surfaces was further confirmed by AFM measurements, which also revealed the morphology of surfaces and the root-mean-square roughness had increased from ~ 1.4 nm to ~ 1.7 nm (Fig. 2c). XPS analysis was performed to confirm the binding of **6** to the Au film. A comparison between the XPS spectra of bare Au film and **6** coated Au film for the binding energy of C 1*s* core level electrons and Au 4*f* core level electrons has been done. The C 1*s* spectrum for bare Au film was fitted with the single peak centered at 284.6 eV. On the other hand, C 1*s* spectrum of **6** coated Au film was best fitted with two peaks centered at 284.6 and 286.7 eV. These peaks were assigned to hydrocarbons (C-C/C-H, 284.6 eV) and ether/alcohol carbon (C-O-X, 286.7 eV) of **6** molecules present onto the Au film.

Entry	Type of coverage on Slides	Contact angle (°) (Conc 6)	Ellipsometry (Å)	Conc of Mannose (µg/cm^2) (conc 6)
1	Au + **6**	85 ± 2 (0.2 M) 78 ± 2 (0.02 M) 64 ± 2 (0.005 M)	13.9 ± 0.172 [39]	-
2	Au + **6** + **M-1** (10 µM)	71 ± 2 (0.2 M) 33 ± 2 (0.02 M) 49 ± 2 (0.005 M)	29.82 ± 0.129	0.2 ± 0.01 (0.2 M) 1.9± 0.01 (0.02M) 1.3 ± 0.03 (0.005 M)
3	Au + **6** + **M-1**+ **Con A**	Not measured	92.93 ± 0.794	-

Table 1. Contact angle and length of monolayer measured in ellipsometry. Conc **M-1** = 10 µM and Conc **Con A** =1 mg/1 ml.

Figure 3b shows that Au 4*f* spectrum for the bare Au film was resolved in two peaks situated at 84.6 and 88.2 eV for Au 4*f*7/2 (Au^0) and Au 4*f*5/2 (Au^0). On the contrary, Au 4*f* spectrum for **6** coated Au film was deconvoluted in four peaks, centered at 83.3, 84.6, 86.9 and 88.2 eV, attributed to Au 4*f*7/2 (Au^0), Au 4*f*7/2 (Au-S), Au 4*f*5/2 (Au^0) and Au 4*f*5/2 (Au-S), respectively (fig. 3d)The chemical shift of 1.3 eV towards the low binding energy in the Au 4*f*7/2 (Au^0) and Au 4*f*5/2 (Au^0) peaks, and appearance of Au 4*f*7/2 (Au-S) and Au 4*f*5/2 (Au-S) peaks after **6** deposition confirms the binding of **6** to the Au film (fig. 3).

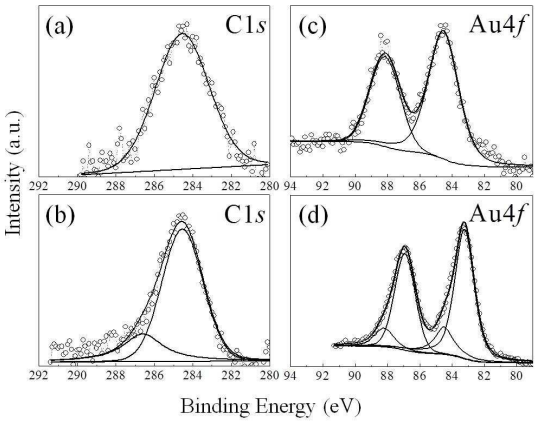

Fig. 3 XPS spectra of (a) C 1*s* for bare Au film, (b) C 1*s* for **6** coated Au film, (c) Au 4*f* for bare Au film (d) Au 4*f* for **6** coated Au film.

After assessing the structure of the gold substrates, we used them for investigating multivalent carbohydrate–protein interactions. The lectin Concanavalin A (**Con A**) served as model for these studies since it selectively binds to *α*-mannopyranosides. **Con A** molecules were immobilized on the substrates by immersing the **6/M-1** coated slides in **Con A** solution (1 mg/1 ml in HEPES) for 1 hour, followed by washing with water. Ellipsometry measurements revealed a very strong increase in the thickness of the layers, ~92.93 Å as compared to ~29.82 Å (Table 1 Entry 3, Fig. S1, S1d & 1h) and R value was found to be ~4.2 nm (Fig. 2d). The large increase in the height is indicative of the immobilization of the proteins on the gold substrates.[40] In order to assess the protein-carbohydrate interactions; we studied their surface Plasmon resonance (SPR) measurements with **Con A** lectin. The cyclodextrin scaffolds (**M-1, M-**

2 and β-CD) on Comp **6** were immobilized on the gold chip before the solutions of different concentrations of **Con A** (0 to 3.5 µM) were flowed over the chip.

Before conducting the carbohydrate-protein interactions, the host-guest properties of Compound **6** and **β-CD** were confirmed. Two different concentrations of **6** was immobilized on the gold coated SPR sensor chips to generate low-density (**6**-LD**, 0.01 mM**) and high-density (**6**-HD**, 0.1 mM**) adamantane surfaces. SPR and kinetic analyses were based on a 1:1 interaction model. The SPR analyses of high and low density of adamantane showed marginal difference in binding affinity (Table 2, Fig. S2)**,** indicating that the concentration of adamantane backbone is critical for host-guest interactions as reported by park et al.[39] Based on the above results, we constructed four host-guest complexes of **6** and **M-1 (H-1, H-2, H-3, and H-4)** at an optimal concentration useful for **Con A** binding and then studied how multivalency and host-guest interactions were influencing the carbohydrate-protein interactions (fig. 4). In case of **H-1** and **H-2**, the density of adamantly linker **6** was maintained low (0.01 mM) and **M-1** concentration was increased to 5 and 50-folds with respect to **6**, resulting in optimum host-guest interaction. Whereas, in case of **H-3** and **H-4**, the density of **6** was high (0.1 mM) and close proximity of the group results weak host-guest complexes, result low sugar density on the surface. The SPR analyses of these four mannose surfaces with different concentration of **Con A** revealed that **H-2** binds 2-fold strongly as compared to **H-1**, a similar experiment with **H-3 and H-4** displayed almost identical binding and displayed much weaker binding compared to **H-2.** Overall, these results are comparable with reported values.[41-42] On the basis of these results, we hypothesized that at low density of **6**, adamantane groups are well separated to host substantial amount of **M-1** to increase the **Con A** binding**.** On the other hand, the large number of **M-1** also restricts **ConA** interaction to 2-fold increase**.** At high density of **6**, the close proximity of adamantane groups restricts hosting of **M-1** moieties to increase the binding affinity. To confirm the influence of hepta-valent sugar topology, we performed the SPR experiments with four different concentrations of **6** and **M-2** (**H-5, H-6, H-7** & **H-8**) complexes (fig. S3). SPR analyses revealed weak association and dissociation constant as compared to **H-2**. The K_d value of **H-5** to **H-8** are comparable to monovalent mannose-**Con A** binding affinity. [41,43] This outcome clearly showed that spatial arrangement of hepta-valent sugar on **β–CD** not only increases the sugar density, but also increases the binding interactions (Fig. 4, S3, Table 2). Finally, to confirm the role of **β–CD** in carbohydrate-protein interactions, SPR analysis of **6/β–CD** complex (**H-9** & **H-10**) was carried out. As expected, **β–CD** complex showed a weak binding with **Con A** lectin (Fig. S4 and table 2).

Together these results show that, in the context of a host-guest multivalent platform, the strength of the binding interactions between **Con A** and mannose directly correlates with spatial arrangement of mannose-capped- **β–CD**.[44] Similar experiments with **H-1** and **H-2** complex with PNA (galactose specific lectin) revealed no binding, proving the specificity (Fig. S5 and Table 2).

A possible application of our system composed of mannose capped **β–CD** that interact strongly with lectin was illustrated by the adhesion of THP-1 differentiated macrophage cells on the gold coated glass surfaces. Macrophage cells are reported to have C-type lectin receptors that recognize high-mannose glycans.[45] Previously, multivalent mannosylated **β-CD** scaffolds have been well characterized towards binding macrophage mannose receptor.[46] Thus we hypothesized that **6/M-1** could bind macrophages more strongly than **6**/**M-2**. To study this, sugar coated gold slides were constructed using multivalent **6/M-1** and monovalent **6**/**M-2** respectively. The glyco-surfaces were exposed to solutions containing a known number of macrophage cells and incubated for 24 h. After washing with PBS, the slides were exposed for bright microscopic imaging. Maximum numbers of cells were observed on **6**/**M-1**-coated slides (Fig. 5b, S6 & S7).

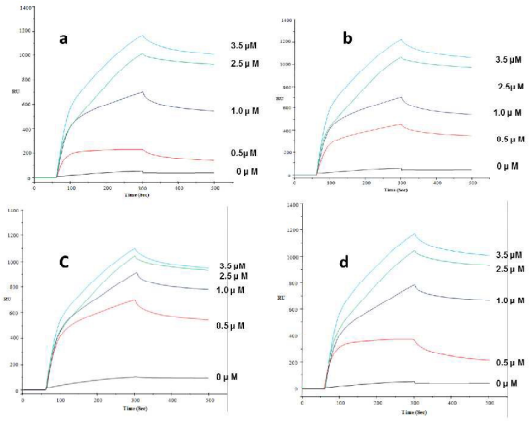

Fig. 4 SPR sensograms for different concentrations of **Con A** incubated with (a) **H-1: 6** (0.01mM) & **M-1** (0.05 mM); (b) **H-2: 6** (0.01 mM) & **M-1** (0.5 mM); (c) **H-3: 6** (0.1mM) & **M-1** (0.05 mM); (d) **H-4: 6** (0.1 mM) & **M-1** (0.5mM).

Table 2 Kinetic parameters for the interaction between **Con A** and mannose- based monovalent and multivalent derivatives.

Composition (mM)		Entry	*vs*	K_A (M^{-1} s^{-1})	K_D (s^{-1})	K_d(M^{-1})
6 (0.01mM)			**β-CD**	1.21 X 10^2	6.15 X 10^{-2}	0.19 X 10^4
6 (0.1mM)			**β-CD**	1.12 X 10^2	4.90 X 10^{-2}	0.23 X 10^4
6 (0.01mM)	**M-1** (0.05mM)	**H-1**	**Con A**	1.14 X 10^6	2.22 X 10^{-5}	0.55 X 10^{11}
	M-1 (0.5mM)	**H-2**	**Con A**	2.67 X 10^6	2.20 X 10^{-5}	1.21 X 10^{11}
6 (0.1mM)	**M-1** (0.05mM)	**H-3**	**Con A**	3.55 X 10^5	1.69 X 10^{-5}	0.21 X 10^{11}
	M-1 (0.5mM)	**H-4**	**Con A**	5.35 X 10^5	1.49 X 10^{-5}	0.36 X 10^{11}
6 (0.01mM)	**M-2** (0.05mM)	**H-5**	**Con A**	1.38 X 10^4	3.04 X 10^{-4}	0.45 X 10^8
	M-2 (0.5mM)	**H-6**	**Con A**	1.04 X 10^4	1.01 X 10^{-4}	1.04 X 10^8
6 (0.1mM)	**M-2** (0.05mM)	**H-7**	**Con A**	0.228 X 10^4	1.75X 10^{-4}	0.13 X 10^8
	M-2 (0.5mM)	**H-8**	**Con A**	0.56 X 10^4	2.81 X 10^{-4}	0.19 X 10^8
6 (0.01mM)	**β-CD** (0.05mM)	**H-9**	**Con A**	1.44 X 10^2	3.62 X 10^{-2}	0.439 X 10^4
	β-CD (0.5mM)	**H-10**	**Con A**	1.59 X 10^2	3.76 X 10^{-2}	0.42 X 10^4
6 (0.01mM)	**M-1** (0.05mM)	**H-1**	PNA	-	-	-
	M-1 (0.5mM)	**H-2**	PNA	-	-	-

Whereas **6/M-2** (Fig. 5c & S8) and **6/β–CD** (Fig. 5a & S9) coated surfaces appeared to have less number of bound cells with spherical morphology. Closer examination of **6/M-1** coated slides revealed that most cells have highly spread fashion. The statistical analysis of the complete slides indicated 3-4 fold difference between **6**/**M-1** *vs*

6/M-2 (Fig. 5d). These results indicate that multivalent sugars on **β–CD** increase the local concentration of sugars to influence the avidity of carbohydrate-protein interactions.

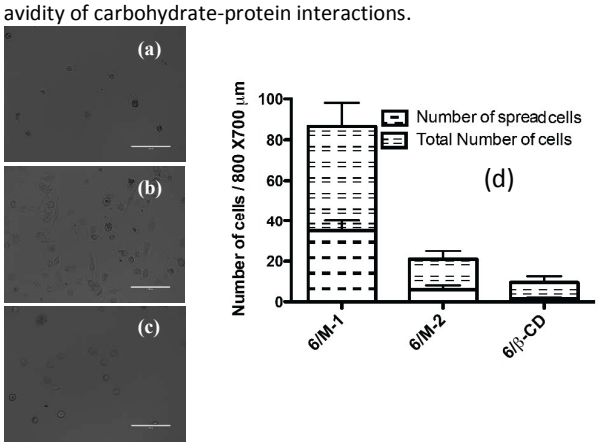

Fig. 5 Representative images of macrophage adhesion to substrates covered with (a) **6/β-CD**, (b) **6/M-1** and (c) **6/M-2** after 24 hour incubation. Scale bar length is 200 µm. (d) Quantitative analysis of macrophage adhesion after 24 h incubation.

Conclusions

We have developed a technique for immobilizing multivalent carbohydrates on surfaces that is based on self-assembly-driven host-guest interactions between **β-CD** and adamantane molecules. This approach is simple, sensitive, and applicable for the study of carbohydrate-protein and carbohydrate-cell interactions using surface bound sugars. This strategy enables one to explore the significance of spatial arrangements of sugars on the surfaces for the interaction with lectins and to probe the role of monovalent sugar *vs* multivalent sugar immobilization. In addition, it can be used for high throughput, reversible and sensitive carbohydrate based biomedical devices.

Acknowledgements

‡ R. K. and M. G. thank IISER Pune, Indo-German (DST-MPG) program, DAE (Grant No.2011/37C/20/BRNS) and UGC India for financial support.

References

1 K. Drickamer, M. E. Taylor, *Annu. Rev. Cell. Biol*., 1993, **9**, 237-264.
2 H. Lis, N. Sharon, *Chem. Rev*., 1998, **98**, 637-674.
3 F. T. Liu, *Clin, Immunol*., 2000, **97**, 79-88.
4 P. H. Seeberger, D. B. Werz, *Nat. Rev. Drug. Discov*., 2005, **4**, 751-763.
5 M. Paolino, L. Mennuni, G. Giuliani, M. Anzini, M. Lanza, G. Caselli, C. Galimberti, M. C. Menziani, A. Donati, A. Cappelli, *Chem. Commun.,* 2014, **50**, 8582-8585.
6 C. Fasting, C. A. Schalley, M. Weber, O. Seitz, S. Hecht, B. Koksch, J. Dernedde, C. Graf, E. W.Knapp, R. Haag, *Angew. Chem. Int. Ed.,* 2012, **51**, 10472–10498.
7 L. L. Kiessling, J. E. Gestwicki, L. E. Strong, *Angew. Chem. Int. Ed.,* 2006, **45**, 2348–2368.
8 S. M. Dimick, S. C. Powell, S. A. McMahon, D. N. Moothoo, J. H. Naismith, E. J. Toone, *J. Am. Chem. Soc.,* 1999, **121***,* 10286-10296.
9 M. Paolino, H. Komber, L. Mennuni, G. Caselli, D. Appelhans, B. Voit, A. Cappelli, *Biomacromolecules,* 2014, **15**, 3985−3993.
10 S. Galeazzi, T. M. Hermans, M. Paolino, M. Anzini, L. Mennuni, A. Giordani, G. Caselli, F. Makovec, E. W. Meijer, S. Vomero, A. Cappelli, *Biomacromolecules*, 2010, **11**, 182–186.
11 A. Martinez, C. O. Mellet, J. M. G. Fernandez, *Chem. Soc. Rev*., 2013, **7**, 4746-4773.
12 J. L. J. Blanco, C. O. Mellet, J. M. G. Fernandez, *Chem. Soc. Rev*., 2013, **7**, 4518-4531.
13 K. Hatano, K. Matsuoka, D. Terunuma, *Chem. Soc. Rev*., 2013, **7**, 4574-4598.
14 C. Fasting, C. A. Schalley, M. Weber, O. Seitz, S. Hecht, B. Koksch, J. Dernedde, C. Graf, E. W. knapp, R. Haag, *Angew. Chem. Int. Ed*., 2012, **15**, 10472-10498.
15 S. Park, J. C. Gildersleev, O. Blixt, I. Shin, *Chem. Soc. Rev*., 2013, **42**, 4310-4326.
16 T. Horlacher, P. H. Seeberger, *Chem. Soc. Rev*., 2008, **37**, 1414-1422.
17 D. Wang, S. Liu, B. J. Trummer, C. Deng, A. Wang, *Nat. Biotechnol*., 2002, **20**, 275-281.
18 K. A. Barth, G. Coullerez, L. M. Nilsson, R. Castelli, P. H. Seeberger, V. Vogel, M. Textor, *Adv. Funct. Mat*., 2008, **18**, 1459-1469.
19 S. N. Narla, X. L. Sun, *Biomacromolecules*, 2012, **13**, 1675-1682.
20 M. R. Lee, I. Shin, *Org. Lett.*, 2005, **7**, 4269-4272.
21 S. Park. M. R. Lee, I. Shin, *Bioconjug. Chem*., 2009, **20**, 155-162.
22 Z. Pei, H. Yu, M. Theurer, A. Walden, P. Nilsson, M. Yan, O. Ramstrom, *ChemBioChem*, 2007, **8**, 166-168.
23 S. Park, M. R. Lee, S. J. Pyo, I. Shin, *J. Am. Chem. Soc*., 2004, **126,** 4812-4819.
24 Y. Zhang, C. Campbell, Q. Li, J. C. Gildersleeve, *Mol. BioSyst*., 2010, **6,** 1583-1591.
25 C. Y. Huang, D. A. Thayer, A. Y. Chang, M. D. Best, J. Hoffmann, S. Head, C. H. Wong, *Proc. Natl. Acad. Sci. USA*., 2006, **103,** 15-20.
26 K. Godula, D. Rabuka, K. T. Nam, C. R. Bertozzi, *Angew. Chem. Int. Ed*., 2009, **48,** 4973-4976.
27 M. Kohn, R. Wacker, C. Peters, H. Schroeder, L. Soulere, R. Breinbauer, C. M. Neimeyer, H. Waldmann, *Angew. Chem. Int. Ed*., 2003, **42,** 5830-5834.
28 Y. Sato, K. Yoshioka, T. Murakami, S. Yoshimoto, O. Niwa, *Langmuir*, 2012, **28**, 1846-1851.
29 M. Paolino, F. Ennen, S. Lamponi, M. Cernescu, B. Voit, A. Cappelli, D. Appelhans, H. Komber, *Macromolecules,* 2013, **46**, 3215−3227.
30 L. Voskuhl, C. Wendeln, F. Versluis, E. C. Fritz, O. Roling, H. Zope, C. Schulz, S. Rinnen, H. F. Arlinghaus, B. J. Ravoo, A. Kros, *Angew. Chem. Int. Ed.,* 2012, **51**, 12616-12620.
31 D. Dorokhin, S. H. Hsu, N. Tomczak, C. Blum, V. Subramaniam, J. Husken, D. N. Reinhoudt, A. H. Velders, G. J. Vancso, *Small*, 2010, **6,** 2870-2876.
32 A. G. Campo, S. H. Hsu, L. Puig, J. Huskens, D. N. Reinhoudt, A. H. Velders. *J. Am. Chem. Soc*., 2010, **132**, 11434-11436.
33 L. Yang, A. G. Casado, J. F. Young, H. D. Nguyen, J. C. Danes, J. Huskens, L. Brunsveld, P. Jonkheijm, *J. Am. Chem. Soc*., 2012, **134,** 19199-19206.
34 C. A. Nijhuis, J. K. Sinha, G. Wittstock, J. Huskens, B. J. Ravoo, D. N. Reinhoudt, *Langmuir,* 2006, **22**, 9770-9775.

35 M. Gade, A. Paul, C. alex, D. Choudhury, H. V. Thulasiram, R. Kikkeri, *Chem. Commun*., 2015, **51**, 9185-9187.
36 Q. Zhenhui, P. Bharate, H. L. Chian, Z. Benjamin, B. Christoph, S. Andrea, B. Fabian, H. Benjamin, M. Rolf, P. H. Seeberger, H. Rainer, *Nano Lett.,* 2015, **15**, 6051−6057.
37 A. G. Barrientos, J. J. G. Lopez, J. I. Garcia, F. O. Caballero, U. Uriel, A. V. Berenguel, F. S. Gonzalez, *Synthesis,* 2001, 1057-1064.
38 F. Vitale, I. Fratoddi, B. Battocchio, E. Piscopiello, L. Tapfer, M. V. Russo, G. Polzonetti, C. Giannini, *NanoScale Res. Lett*., 2011, **6**, 103-111.
39 J. H. Park, S. Hwang, J. Kwak, *ACS Nano*, 2010, **4**, 3949-3958.
40 P. N. Kanellopoulos, K. Pavlou, A. Perrakis, B. Agianian, C. E. Vorgias, C. Mavrommatis, M. Soufi, P. A. Tucker, S. J. Hamodrakas, *J. Struct. Biol*., 1996, **116,** 345-355.
41 W. Vornholt, M. Hartmann, M. Keusgen, *Biosensor Biolelectron.,* 2007, **22**, 2983-2988.
42 T. Mori, M. Toyoda, T. Ohtsuka, Y. Okahata, *Anal. Biochem*. 2009, **395**, 211-216.
43 G. Bellapadrona, A. b. Tesler, D. Grunstein, L. H. Hossain, R. Kikkeri, P. H. Seeberger, A. Vaskevich, I. Rubinstein, *Anal. Chem.,* 2012, **84**, 232-240.
44 D. Grunstein, M. Maglinao, R. Kikkeri, M. Collot, K. Barylyuk, B. Lepenies, F. Kamena, R. Zenobi, P. H. Seeberger, *J. Am. Chem. Soc.,* 2011, **133,** 13957-13966.
45 T. E. Wileman, M. R. Lennartz, P. D. Stahl, *Proc. Natl. Acad. Sci. USA*., 1986, **83**, 2501-2505.
46 J. M. Benito, M. G. García. C. O. Mellet, I. Baussanne, J. Defaye, J. M. G. Fernandez, *J. Am. Chem. Soc*., 2004, **126**, 10355-10363.